Manuscript prepared for Atmos. Chem. Phys.
with version 3.2 of the LaTeX class copernicus.cls.
Date: 4 November 2014

The use of SMILES data to study ozone loss in the Arctic winter 2009/2010 and comparison with Odin/SMR data using assimilation techniques

Kazutoshi Sagi[1], Donal Murtagh[1], Joachim Urban[†,1], Hideo Sagawa[2], and Yasuko Kasai[2]

[1]Department of Earth and Space Sciences, Chalmers University of Technology, Gothenburg, Sweden
[2]National Institute of Information and Communications Technology, Tokyo, Japan
[†]Deceased 14 August 2014

Correspondence to: Kazutoshi Sagi
sagi@chalmers.se

Abstract. The Superconducting Submillimeter-Wave Limb-Emission Sounder (SMILES) on board the International Space Station observed ozone ~~profiles~~ in the stratosphere with high precision from October 2009 to April 2010. Although SMILES measurements only cover latitudes from 38°S to 65°N, the combination of data assimilation methods and an isentropic advection model allows us to use SMILES measurements to investigate the ozone loss by making use of the instability of the polar vortex in the northern hemisphere. We quantified the ozone depletion in the 2009/2010 Arctic polar winter. Ozone data from both SMILES and Odin/SMR (Sub-Millimetre Radiometer) for the winter were assimilated into the Dynamical Isentropic Assimilation Model for OdiN Data (DIAMOND). DIAMOND is an off-line wind-driven transport model on isentropic surfaces. Wind data from the operational analyses of the European Centre for Medium- Range Weather Forecasts (ECMWF) were used to drive the model. In this study, particular attention is paid to the cross isentropic transport of the tracer in order to accurately assess the ozone loss. The assimilated SMILES ozone fields agree well with the limitation of noise induced variability with the SMR fields despite the limited latitude coverage of the SMILES observations. Ozone depletion has been derived by comparing the ozone field acquired by sequential assimilation with a passively transported ozone field initialized on 1 December 2009. Significant ozone loss was found in different periods and altitudes from using both SMILES and SMR data: The initial depletion occurred at the end of January below 550K with an accumulated loss of 0.6 - 1.0 ppmv (approximately 20 %) by 1 April. The ensuing loss started from the end of February between 575K and 650K. Our estimation shows that 0.8–1.3 ppmv (20 – 25 %) of O_3 has been removed at the 600K isentropic level by 1 April in VMR.

1 Introduction

According to many studies of stratospheric ozone (O_3) ~~over the Antarctic~~, major ozone depletion inside the isolated polar vortex is caused by the formation of Polar Stratospheric Clouds (PSC) and the associated heterogeneous release of active chlorine species (Cl, ClO) (e.g. Solomon, 1999). However, in comparison with the Antarctic polar vortex, the Arctic vortex is less stable due to the propagation of planetary waves from the troposphere. Therefore, the periods during which the temperature inside vortex goes below the threshold for PSC formation are limited (WMO, 2011). These effects make the quantification of chemical ozone depletion in the Arctic generally more difficult.

The winter of 2009-2010 was colder than other winters in the last decade during January (e.g. Dörnbrack et al., 2012). Figure 1 indicates the minimum temperature (T_{min}) as a function of days of the year (DOY) derived from the European Centre for Medium-range Weather Forecasts (ECMWF) operations on the 500 K potential temperature (PT) surface at equivalent latitudes (EQL) greater than 70°N. The T_{min} for the winter period of 2009-2010 was lower than 185 K from 1 January and became as low as 180K on 7 January (see also Dörnbrack et al., 2012). This temperature behavior has been presented previously. Khosrawi et al. (2011) reported that strong denitrification caused by the formation of the PSCs was observed during the synoptic cooling event in mid-January 2010. However, a Sudden Stratospheric Warming (SSW) ended the coldest period after 19 January (Dörnbrack et al., 2012; Kuttippurath and Nikulin, 2012). SSWs are wintertime phenomena that are characterized by suddenly increasing temperatures and a reversal of the zonal wind (Scherhag, 1952). The planetary wave disturbance of the vortex with the occurrence of the SSW event makes this winter dynamically complicated.

SMILES (Superconducting Submillimeter-wave Limb-Emission Sounder), a passive atmospheric sensor attached to the Japanese Experiment Module (JEM) on board the International Space Station (ISS), was developed by the Japan Aerospace Exploration Agency (JAXA) and the National Institute of Information and Communications Technology (NICT). SMILES used a 4K superconducting detector technology to measure high precision vertical profiles of stratospheric and mesospheric species related to ozone chemistry. The instrument was operated from October 2009 until April 2010 when the local oscillator failed providing atmospheric composition data typically within the latitude range of 38°S-65°N (Kikuchi et al., 2010).

The subject of this paper is to demonstrate the use of the high sensitivity observations by SMILES to quantify polar ozone loss. However, it is still a challenge to use SMILES data to analyze the polar regions because of its limited latitude coverage. The Odin/SMR ozone has been also analyzed in this study for comparison with SMILES ozone because this instrument also uses the limb sounding technique and has a long record of stratospheric ozone measurements starting in 2001. Figure 2 shows a typical observation map of SMILES and SMR and Table 1 summarizes the nominal specification of both observations. The higher vertical scan rate of SMILES compared to SMR

explains the larger number of measurements. In addition, the dynamical instability of this winter season, displacing the vortex to latitudes below 65°N, permitted a considerable number of SMILES observations within the vortex. Thus SMILES made more measurements than SMR even in the vortex (EQL≥70°N) (see Fig. 3). On the other hand, there are periods when SMILES measurements inside the vortex were not available due to ISS maneuvers. In the first half of December, the field of view of the SMILES antenna was blocked by the ISS solar paddles ~~at high latitudes~~, resulting only in a few useable measurements. Another ~~empty~~ period without measurements, in the middle of February, is due to the rotation of the ISS to dock with the space shuttle Endeavour. When the space shuttle was docked, the ISS was rotated by 180° and SMILES looked towards the southern hemisphere.

In this paper, we employed the data assimilation technique developed for other Arctic winters by Rösevall et al. (2007a,b, 2008) to investigate the ozone depletion in the 2009/2010 winter using SMILES ozone data. Other similar studies have used various models and assimilation methods (El Amraoui et al., 2008; Jackson and Orsolini, 2008; Søvde et al., 2011). One advantage of data assimilation is that it allows us to optimally use all measurements and is useful for interpolating or extrapolating the ozone distributions when and where no measurements are available. In this study we have ~~also~~ used the DIAMOND assimilation model developed by Rösevall et al. (2007b) to produce active and passive tracer fields. However, because it is a two-dimensional model, Rösevall et al. (2007a,b, 2008) needed to account for the effect of the diabatic descent inside the vortex a posteriori. Thus we have implemented a new vertical transport scheme that continuously accounts for the descent rather than an a-posteriori correction. Ozone observed by SMR is ~~also~~ analyzed for comparison. This paper is structured as follows. Sections 2 and 3 describe the measurements and the model, respectively. Section 4 tests the effectiveness of the new vertical transport scheme using the long lived species N_2O measured by SMR and then shows the results of the ozone analyses. Finally, we conclude the study in section 5.

2 Measurement descriptions

Profiles of ozone were obtained from the SMILES and SMR instruments. Nitrous oxide (N_2O) from SMR was ~~also~~ used for this study ~~. N2O gnerally used~~ as a tracer of transport in the stratosphere due to its long lifetime for checking the dynamics in the model.

2.1 SMILES

SMILES observed atmospheric limb emissions from the ISS flying at an altitude of ∼340 – 360 km. It vertically scanned the tangent heights of ∼ -20 – 120 km with an antenna field-of-view of ∼3 km. A single spectrum was obtained with a data integration time of 0.47 s, and one vertical scan took 53 s including the calibration data acquisition. About 1630 scans were obtained per day. Because the

ISS has a non sun-synchronous orbit, the local time of SMILES measurement location evolved over 24 hour after approximately 1 month.

SMILES operated in three frequency bands: 624.32 – 625.52 GHz (band A), 625.12 – 626.32 GHz (band B), and 649.12 – 650.32 GHz (band C). Bands A and B contain the emission line of ozone at 625.371 GHz. ~~SMILES detected the submillimeter emission of ozone at 625.371 GHz. There are three instrumental configurations for the SMILES ozone 625.371 GHz observations: two different observation frequency bands (named band-A and B hereafter) and two different AOS units.~~ The ~~spectra~~ measurements are spectrally resolved with an Acousto-Optical Spectrometer (AOS) which has a bandwidth of 1.2 GHz and a resolution of 1.2 MHz. Since SMILES only had two AOSs, the bands were observed on a time-sharing basis. The measurement noise of SMILES is as low as $<$ 0.7 K (for a single AOS channel and a single spectrum) due to the low noise performance of the superconductor-insulator-superconductor (SIS) mixers. See Kikuchi et al. (2010) for further details about the SMILES instrumentation.

We used the ozone data processed by the NICT level-2 chain version 2.1.5. This level-2 ~~chain~~ algorithm employs a least-squares method with a priori regularization (e.g. Rodgers, 2000) as described by Baron et al. (2011). The SMILES NICT ozone data was validated in Kasai et al. (2013). The SMILES ozone profile covers altitudes from 16 to 90 km with a resolution of $\sim$3 - 4 km ~~and $\sim$6 - 10 km for~~ in the stratosphere ~~and mesosphere, respectively~~.(see Fig. 2 in Kasai et al., 2013). Based on the error analysis and comparison studies of ~~mid-latitude ozone data~~, Kasai et al. (2013) reported a systematic error of better than 0.3 ppmv in the stratosphere ($\sim$60 - 8 hPa). The random error for a single ozone profile is as low as 1% for this altitude region. It is also reported that the data quality of ozone profiles from band-B is better than that from band-A. Ozone data from both bands are used in this study since no bias exists between ozone from band A and B (see Kasai et al., 2013). Band A ozone data are only used when data from band B are not available.

2.2 Odin/SMR

Odin is a Swedish satellite mission in association with Canada, Finland and France, which was designed for radio astronomy and limb sounding of the Earth's middle atmosphere (Murtagh et al., 2002). Odin was launched on 20 February 2001 into a sun-synchronous polar orbit with an inclination of 98°, altitude of $\sim$600 km and descending and ascending nodes at 6 and 18 hours local solar time, respectively. It carries two different limb sounding instruments, OSIRIS (Optical Spectrograph/InfraRed Imaging System) and SMR (Sub-Millimetre Radiometer). The SMR instrument, described by Frisk et al. (2003), consists of four tunable single-sideband Schottky-diode heterodyne microwave receivers.

The datasets for ozone and N_2O from SMR used in this paper are products of the stratospheric mode that is operated every other day since April 2007 (every third day previous to this). In the stratospheric observation mode, two of the receivers, covering the bands centered at 501.8 GHz and

544.6 GHz, are used for detecting the spectral emission lines of ozone, N_2O, ClO and HNO_3. The ozone and N_2O profiles used in this study are retrieved from emission lines at 501.5 GHz and 502.3 GHz, respectively, using the Chalmers version 2.1 retrieval scheme.

The SMR ozone profiles cover the altitude range ∼17–50 km with an altitude resolution of 2.5–3.5 km and an estimated single-profile precision of ∼1.5 ppmv (Urban et al., 2005a). SMR v2.1 ozone data has been validated against balloon sonde measurements as described in detail by Jones et al. (2007). It shows that SMR ozone in the 60°N–90°N latitude band has mixing ratios that are 0.0–0.1 ppmv lower than sonde measurements below 23 km and a positive bias of SMR ozone 0.1–0.3 ppmv in the 23 to 30 km range. The validation study (Kasai et al., 2013) shows that SMILES generally gives slightly lower ozone values than SMR at altitudes below 20 hPa.

The N_2O profiles cover altitudes in the range 12–60 km with an altitude resolution of ∼1.5 km. The estimated systematic error is less than 12 ppbv (Urban et al., 2005a). The validation of the N_2O is reported by Urban et al. (2005b). Further comparisons with the Fourier Transform Spectrometer (FTS) onboard the Atmospheric Chemistry Experiment (ACE) and the Microwave Limb Sounder (MLS) on the Earth Observing System (EOS) Aura satellite are shown by Strong et al. (2008) and Lambert et al. (2007), respectively. SMR N_2O agrees with ACE/FTS N_2O within 7% between 15 and 30 km (Strong et al., 2008). And SMR N_2O v2.2 is larger than MLS N_2O by ∼5% in the pressure range of 68 – 4.6 hPa and 10% larger at 100 hPa (Lambert et al., 2007).

3 DIAMOND model

The DIAMOND (Dynamic Isentropic Assimilation Model for OdiN Data) ~~model~~ is an off-line wind driven isentropic transport and assimilation model designed to simulate quasi-horizontal ozone transport in the lower stratosphere with low numerical diffusion. Isentropic off-line wind driven advection has been implemented using the second order momentum (SOM) advection scheme (Prather, 1986) which is a mass conservative Eulerian scheme. The idea of the Prather scheme is that by preserving the zero to second order moments of the sub-grid scale tracer distribution the quality of the transport is preserved. In this study, the wind fields from the operational analyses of the ECMWF have been used. Advection calculations are performed on separate layers with ~~a~~ constant potential temperature (PT) ranging from 400 K to 1000 K in 25 K intervals.

The tracer profiles from SMILES or SMR are sequentially assimilated into the advection model. The assimilation scheme in DIAMOND is described as a variant of the Kalman filter. Details on the assimilation scheme can be found in Rösevall et al. (2007b).

3.1 Cross-isentropic Transport

Under adiabatic conditions, PT is conservative in dry air and thus the air parcels normally move on a constant PT surface. ~~However, there is a strong descent inside the vortex due to the radiative cooling~~

~~during the polar night.~~ ~~Thus, quantification of diabatic vortex descent is necessary to correctly evaluate the ozone loss.~~ The descent of air in the polar vortex caused by radiative cooling during polar night had not be taken into account in the previous model version. It is, however, necessary for a correct evaluation of ozone loss.

For a flow field (u,v,w), the advection equation of a (passive or active) tracer $\Psi(x,y,\Theta,t)$ at given horizontal coordinates x and y, vertical coordinate in potential temperature Θ and time t in an Eulerian coordinate system is:

$$\frac{\partial\psi}{\partial t} = -u\frac{\partial\psi}{\partial x} - v\frac{\partial\psi}{\partial y} - w\frac{\partial\psi}{\partial\Theta}. \tag{1}$$

Here, u and v are the horizontal wind speeds. w is the vertical component of air mass advection with units of K/day. As we mentioned previously, DIAMOND employs the SOM method to solve the first and second terms on the right hand side in equation 1. On the other hand to account for the descent we ~~on the other hand~~ implemented a simple vertical transport scheme into DIAMOND. The following equation is the one dimensional first-order upstream method implemented into the model,

$$\frac{(\Psi(\Theta,t+\Delta t)-\Psi(\Theta,t))}{dt} = \underline{w}\frac{(\Psi(\Theta-\Delta\Theta,t)-\Psi(\Theta,t))}{d\Theta}$$
$$\Psi(\Theta,t+\Delta t) = \Psi(\Theta,t)\left(1-\underline{w}\frac{dt}{d\Theta}\right) + \Psi(\Theta-\Delta\Theta,t)\underline{w}\frac{dt}{d\Theta}. \tag{2}$$

The first-order upstream method often produces numerical diffusion. In order to avoid this, it is at least necessary to satisfy the following condition,

$$\frac{\Delta\Theta}{\Delta t} > C \tag{3}$$

where $\Delta\Theta$, Δt and C represent the grid interval, the time step and the speed of the phenomenon, respectively. The $\Delta\Theta/\Delta t$ in the model (= 2.5 K/min) is much larger than the general descent rate inside the polar vortex ($\sim$1 K/day), and therefore the first-order upstream method can be used satisfactorily. It is also important to have a sufficiently small separation of the layers to obtain a good representation of the descent.

To quantify the vertical transport, we used the diabatic heating rate Q [K/sec] derived from SLIMCAT 3d chemical transport model calculations (Chipperfield, 2006). The vertical velocity w was calculated as,

$$w = \left(\frac{\Theta}{T}\right)\cdot Q \tag{4}$$

where, ~~Θ and T are potential and~~ T is the absolute temperature~~, respectively~~.

4 Results

4.1 Dynamics of the Arctic winter 2009-2010

In order to test the performance of the model and study the dynamics of this winter, we modelled stratospheric N_2O fields by assimilation of SMR N_2O. A summary of the calculations is given in Table 2. Initialization (i.e. the spin up calculations with assimilations) for one month prior to the investigation period (from 1 December to 31 March) is required to ensure the accuracy of the initial model field. In order to remove contamination by ~~the~~ erroneous observations, the SMR data is used only if the measurement response is larger than 0.85. The measurement response, the summation of the elements of the rows of the averaging kernel matrix, gives the contribution of the measurement to the retrieved information. To reduce any boundary condition problems realistic tracer fields are required. ~~Boundary layers at PT of 400K and 1000K have also been produced by the assimilation for the analysis period in advance. Assimilated fields at PT of 400K and 1000K have also been produced for the boundary layers for the analysis period.~~ These are used as buffer layers to feed the vertical transport scheme. Note that the measurement response especially for SMR N_2O is generally less than 0.7 at lower altitudes (< 450K). Therefore, we relaxed the measurement response threshold to 0.7 for the boundary layers. In the results, we only show the output of the model from 450K to 900K to avoid boundary effects. The uncertainty of the DIAMOND model due to imperfections in the transport scheme and/or unimplemented chemical processes has to be considered. We set the initial error fields to 30% ~~of the US standard atmosphere~~ of the initial ozone field taken from the ECMWF model, which corresponds to the standard variation of the 40 day prediction without assimilations. The error field grows linearly to this value in 40 days if no measurements are available.

Figure 4 shows the model results for N_2O and the corresponding error fields at 600 K. The polar vortex is clearly seen as the area where the volume mixing ratio of N_2O is low. In the maps the EQL of 70°N, which is used as the vortex boundary, is drawn as the black contour line. The white contour lines denote the Lait's modified potential vorticity of 38 PVU ($1\mathrm{PVU} = 1 \times 10^{-6}\mathrm{Km^2kg^{-1}s^{-1}}$) (Lait, 1994). The modified potential vorticity refers to the reference level 475K. The potential vorticity of 38 PVU is also used for the vortex boundary in other studies (Sonkaew et al., 2013; Hommel et al., 2014). The polar vortex was formed at the beginning of December and stayed at high latitudes for two weeks (DOY -31 to -15) then distorted and split into two parts caused by changes in the wind fields due to a minor SSW in the middle of December ($\sim$-15 DOY). The two separate vortices combined by 17 December. Kuttippurath and Nikulin (2012) have given a detailed analysis of these processes by using the potential vorticity. Our N_2O results are consistent with their findings. After that, the vortex stayed cold and remained pole centered until the major SSW occurred at the end of January 2010 (e.g. Dörnbrack et al., 2012; Kuttippurath and Nikulin, 2012). This period shows the lowest temperatures of this winter at potential temperature of 500K (see Figure 1). The major SSW changed the wind field again: massive inflow of air from the Pacific forced

the vortex to move to middle latitudes with flattening over Eurasia (see for example the Odin/SMR quick look at http://www.rss.chalmers.se/~jo/SMRquicklook/Qsmr-2-1/N2O_5018/gm/). Furthermore, the vortex again split after 10 February. The two parts are reunited on 1 March with entraining of some extra-vortex air. The vortex was then relatively stable for some weeks. Finally, when the polar night ended, the vortex broke and the vortex air horizontally mixed with air from outside (Wohltmann et al., 2013).

To illustrate the advection in the DIAMOND model, we derived the vortex mean of N_2O from the daily fields. Figure 5 shows the mean of the N_2O ~~concentrations~~ volume mixing ratios inside the area where the EQL is equal or greater than 70°. The solid lines in the figure are calculated from the results of assimilation of SMR N_2O. The two dashed lines, red and blue, are the vortex mean of the fields predicted by the advection model using the initial N_2O distribution as of 1 December with and without vertical transport, respectively. If the vertical transport would be perfectly simulated in the model, the predicted and assimilated results should have the same values. Compared to the predictions from the 2D advection scheme, the predictions with the vertical transport scheme shows good agreement with the vortex mean assimilated N_2O field until the final break up of the vortex. The uncertainty of the mean, plotted as the shaded areas in figure 5, is calculated as $\sqrt{\sigma^2 + \hat{E}^2}$. Here σ and $\hat{E}$ are the standard deviation of N_2O inside the vortex and the vortex mean of the error field, respectively. More details of these components can be seen in Figure 6. $\hat{E}$ characterizes the error from the point of view of the instrument. However the dominant factor in the uncertainties is the variability inside the vortex (σ). The temporal evolution of σ allows us to assess the contribution of the (mostly horizontal) mixing. At the end of February ($\sim$ 50 DOY), an exponential increase in σ occurs caused by the breaking of the vortex and associated mixing. This is particularly noticeable at 600K.

4.2 Ozone inside the vortex

Figure 7 and 8 display maps of the results for ozone from the assimilations of data from SMILES and SMR. The results from the two instruments have similar patterns in the ozone maps although those from SMR exhibit more features and larger variations. The reasons for the differences are the number and quality of the measurements. Specifically, SMR has fewer measurements at lower latitudes because of its orbit and has a higher noise level. The SMILES ozone abundance, as expected due to known biases, was approximately 0.1 ppmv lower than SMR ozone below 700K corresponding to 20 hPa in pressure (see Figure 20 in Kasai et al. (2013)). Another important point is the incomplete coverage of the center of the vortex for the SMILES assimilation. As noted in the introduction, SMILES did not observe at higher latitudes than 65 °N. As a result the measurement information on ozone in the polar region is transported from lower latitudes by the model. Thus, when the vortex is stable and well isolated, modeled ozone distributions may deviate from the true atmosphere. This is clearly seen in the SMILES ozone maps at the end of December where higher concentrations

compared to earlier are seen inside the vortex due to the descent from higher levels and the lack of any chemical ozone loss processes in the model.

To avoid the effects of large local variations, we have chosen to use the average for the entire vortex for this study. The sampling issues described above are mitigated by employing a weighted average over the vortex as shown in Figure 9. The weights are given by the estimated model error fields. Note the fact that the vortex mean of the SMILES assimilation thereby emphasizes the contribution near the vortex edge. Vortex averages of ozone from both instruments show similar patterns, especially before the major SSW event at the end of January. Uncertainties in Figure 9 are also calculated using the standard deviation σ and the mean of the error field $\hat{E}$ inside the vortex. Since SMR ozone is much noisier, information on the mixing from the vortex internal variation of the ozone fields σ are masked by the average error fields $\hat{E}$, while for SMILES the total error reflects the variation inside the vortex especially when there are sufficient measurements available.

4.3 Ozone loss quantification

Arctic ozone depletion is estimated by subtracting ozone fields passively transported in the DIAMOND model from the fields with assimilated data. The time evolution of the ozone losses derived from SMILES and SMR are presented in Figure 10a and Figure 10b. ozone losses inferred from the two instruments have similar patterns. The major differences are the loss during the period between 13 January (12 DOY) and 30 January (29 DOY) at 650K in SMILES result and the lower loss value from 17 March (75 DOY) below 500K in SMR result. Because the SMILES results reflect not the pole center but lower latitudes near the vortex edge, the apparent loss (12–29 DOY, 650K) in SMILES is due to an overweighting of the losses near the vortex edge. The reason why SMR loss is lower than SMILES below 500K is because SMR ozone measurements tend to overestimate ozone at these altitudes due to lower sensitivity/measurement response.

The first significant depletion occurred below 550K from January 25 to February 7 (24–37 DOY): this corresponds to the period when the vortex moved towards lower latitudes and becomes exposed to sunlight. The loss rate is approximately 0.06 ppmv/day and accumulated loss of 0.8 ppmv can be seen on 7 February (37 DOY) at 500K. ~~Within two weeks, catalytic ozone depletion reached equilibrium with the photochemical production and the horizontal mixing due to the unstable conditions after the SSW.~~ The second ozone loss period took place from the end of February at the heights between 575K and 650K. This continued ~~even after the vortex break up~~ at a rate of 0.03 $\sim$ 0.04 ppmv/day. Figure 11 presents the accumulated ozone loss as of 28 February 2010 just before the beginning of the second loss. The first loss occurring below about 550K is clearly seen in the profiles of ozone loss as peaks at 500K. The maximum losses derived by SMILES and SMR are 1.0 ppmv and 0.7 ppmv at 525K, respectively. Figure 12 shows on the other hand accumulated loss profiles as of 31 March. The loss values below 550K for both instruments are almost the same with these on 28 Feb. However, the loss profiles are higher than on 28 Feb. at most of altitudes with

the maximum values of 1.1ppmv (SMILES) and 1.3 ppmv (SMR) at 600K. Ozone loss as estimated from SMILES is slightly larger at most levels. It is proposed that the difference in ozone loss between the two instruments is a result of sampling differences. SMILES captures ozone changes near the vortex edge where the area has been more exposed to sunlight while SMR on the other hand represents the loss at the centre of the vortex because of its orbit.

The initial loss from 25 January below 550K can be explained using the classical mechanism related to heterogeneous reactions on PSCs and the chlorine catalytic cycle (Solomon, 1988). ~~Generally, PSCs are classified according to the air temperature above (type I) and below (type II) the water ice frost point (T_{ice}). Type I PSCs mainly consist of particles of Nitric Acid Tri-hydrate (NAT).~~ From mid December until the middle of January, the temperature inside the vortex was cold enough to form PSC. ~~not only for type I but also type II (figure 10f, 10g and 10h).~~ Khosrawi et al. (2011) ~~found that due to an unusually strong synoptic cooling event in mid January, ice particle formation on Nitric Acid Tri-hydrate (NAT) may be a possible formation mechanism causing the denitrification observed in mid January.~~ Vortex average ClO in daytime and nighttime are also presented in the Figure panels (10c and 10d). Here, ClO profiles have been retrieved from the frequency band centered at 501.8GHz of SMR (Urban et al., 2005a). To group ClO into day and night time, we used solar zenith angles (SZA) of 90° and 95° as limits to avoid the twilight. Since the partitioning of ClO/Cl_2O_2 is temperature dependent, the enhancement of nighttime ClO at the end of Jan, is the result of thermal decomposition of Cl_2O_2. The peak of ClO at 475K on 28-29 Janunary corresponds to the rise in temperatures after the SSW. On the other hand, the nighttime ClO increased from 16 Dec. (-15 DOY) in advance of the ozone depletion below 500K with 0.1 ppbv is due to chlorine activation on PSCs. The average of ClO during the period from 16 Jan. (15 DOY) to 15 Feb. (45 DOY) is approximately 0.25 ppbv and includes both activation and thermal decomposition.

~~However, it is difficult to explain the upper-level (575K to 650K) ozone loss from the end of February by only chlorine-related destruction.~~ The upper-level (575K to 650K) ozone loss from the end of February was not due to due to chlorine-related destruction. The second loss is correlated with the sun exposure time inside the vortex (shown in Figure 10e). Nevertheless, the vortex average ClO is still low at around 600K (10c). Similar losses were also found in other warm winters (Konopka et al., 2007; Grooß and Müller, 2007; Jackson and Orsolini, 2008; Søvde et al., 2011). Konopka et al. (2007) discussed that the loss around 650K in 2002/2003 was induced by the catalytic cycles of NO_X transported from the mesosphere and lower latitudes. The available result by Kuttippurath et al. (2010) indicates that the $NO - NO_2$ cycle is dominant in a PSC-free polar stratosphere in the PT range of 600-850K.

4.4 Comparison with other studies

Comparable studies of ozone loss in the winter 2009/2010 based on different analysis methods and measurements were done by Kuttippurath et al. (2010), Wohltmann et al. (2013) and Hommel et al.

(2014). The inferred loss of SMR ozone agrees with loss simulated with the chemical transport model ATLAS by Wohltmann et al. (2013). They find cumulative ozone losses of 0.8–0.9 ppmv at 500K until 2010/03/30 based on a 68.5°N equivalent latitude criteria. Values for SMR in Fig. 12 are 0.5–0.8 depending on the vortex criterion (70°N EQL and 38PVU). SMILES losses are larger at this level (0.8–1.3 ppmv). Ozone loss derived from MLS presented by Wohltmann et al. (2013) agrees with the model results presented here. Kuttippurath et al. (2010) only quantify ozone loss until the end of February because of the tracer uncertainties after the major warming while other studies continued the analyses during March. The maximum loss around 550K derived from their model simulation is 1.1 ppmv at the end of February but the corresponding MLS loss is 1.7 ppmv which is larger than loss derived from MLS data by Wohltmann et al. (2013) (1.4 ppmv at 550K for the end of March). MLS loss at these levels is larger than our estimations based on SMILES and SMR ozone. For comparison, the loss derived from SCIAMACHY observations by Hommel et al. (2014) in a layer of 475–525K is of the order of 1 ppmv which is roughly consistent with our results. Note that Hommel et al. (2014) used the 38PVU criterion for defining the vortex edge.

Considering the potential temperature range of 600–650K, our study find cumulative ozone loss until 31 March 2010 of about 1.0 and 1.3 ppmv derived from SMILES and SMR, respectively. Wohltmann et al. (2013) find a loss of 1.3–1.4 ppmv in their model result and a loss of 1.7 ppmv in MLS data. The analysis of SCIAMACHY data shows losses of 1–1.5 ppmv in the beginning of April (Hommel et al., 2014).

Plausible explanations for differences are instrument sampling differences and the vertical resolutions of the profile measurements. Other possible reasons are the different criteria for defining the vortex edge. We have tested two different vortex criteria. In addition to using the EQL of 70 °N, the modified PV criterion (38PVU) applied in Hommel et al. (2014) has been used for quantifying ozone loss. Major differences between ozone loss derived with the two criteria can be seen around 800K on 28 February in figure 11 and below 550K on 31 March in figure 12. With the modified PV criteria we obtain roughly 0.2 ppmv higher loss above 800K on 28 February in Fig 11. In this height range, N_2O has large variations and the standard deviation of ozone inside the vortex (not shown) is large for the period of the vortex separation. However, there are no differences in ozone loss below 700K where ozone loss generally occurs. For example, figure 4 compares the two vortex edge criteria on the 600K level. A good agreement of the two criteria can be seen until the end of February, but differences are found in March. Differences of ozone loss on 31 March at 500K are approximately 0.3 ppmv. It is thus likely that the air near the vortex edge moderates the loss of ozone using the EQL criteria. The losses derived with two criteria agree still with each other within 10%.

5 Conclusions

Datasets from SMILES and SMR have been used to quantify ozone loss inside the polar vortex for the Arctic winter 2009-2010. The investigation was performed using the DIAMOND data assimilation framework. DIAMOND is an off-line wind-driven transport model advecting air on isentropic surfaces into which we introduced the vertical cross-isentropic transport. Assimilation of SMR N_2O was used to verify the cross-isentropic scheme when using SLIMCAT heating rates to calculate the diabatic descent.

We have demonstrated that indeed SMILES measurements combined with a data assimilation technique can be used to study ozone loss even at higher latitudes than 65° N. Ozone fields from assimilation of SMILES and SMR show similar patterns, although the quality and coverage of measurements caused differences between the ozone fields, especially at lower latitudes. The agreement is also seen in the time evolutions of weighted vortex mean of ozone.

Ozone loss was derived by comparing fields acquired by sequential assimilation with passively transported fields. Significant losses are seen at different altitudes using both SMILES and SMR data and can be explained as follows: (I) Before the major SSW ($\sim$ 21 January), the reasonably stable and isolated polar vortex remained centered around the north pole and cold temperatures allowed the formation of PSCs. (II) The SSW changed the wind field and the inflow of air from the Pacific pushed the vortex out towards middle latitudes. (III) The first rapid ozone depletion occurred below 550K mostly close to the vortex edge where the polar night had ended (from January 24th to February 7th). The depletion of $\sim$ 1.0 ppmv is considered to be a result of ClO catalytic destruction. (IV) The second loss of in the height range 575K to 650K started from the end of February and continued until the vortex break up. 20–25% of ozone was removed from this altitudes. This loss was ~~probably~~ induced by the NO_X reactions (Kuttippurath et al., 2010; Sonkaew et al., 2013). Further study is required to fully understand the mechanisms. The accumulated ozone loss as of 28 February derived from SMILES was higher than that from SMR by $< 10\,\%$ and it can be attributed to loss occurring near the vortex edge. The initial peak of ozone loss at lower levels was 0.7 ppmv (15 – 20 %) at 475K for SMR ozone and 1 ppmv (20 – 25 %) at 500 K for SMILES ozone, respectively. The second loss at 600 K was 0.8 ppmv (15 – 20 %) for both instruments. Ozone loss derived using the modified PV criterion agrees with the loss using EQL criterion until the end of February below 700K. Loss with the modified PV criterion on 31 March 2010 is approximately 0.3 ppmv higher at 500K. Our estimation shows lower ozone loss than losses derived from other studies using MLS and SCIAMACHY measurements.

Acknowledgements. We thank Martyn Chipperfield and Wuhu Feng at the University of Leeds for providing the diabatic heating rate for this study and the Swedish National Space Board (SNSB) for funding.

References

Baron, P., Urban, J., Sagawa, H., Möller, J., Murtagh, D. P., Mendrok, J., Dupuy, E., Sato, T. O., Ochiai, S., Suzuki, K., Manabe, T., Nishibori, T., Kikuchi, K., Sato, R., Takayanagi, M., Murayama, Y., Shiotani, M., and Kasai, Y.: The Level 2 research product algorithms for the Superconducting Submillimeter-Wave Limb-Emission Sounder (SMILES), Atmos. Meas. Tech., 4, 2105–2124, doi:10.5194/amt-4-2105-2011, http://www.atmos-meas-tech.net/4/2105/2011/, 2011.

Chipperfield, M. P.: New version of the TOMCAT/SLIMCAT off-line chemical transport model: Intercomparison of stratospheric tracer experiments, Q. J. Roy. Meteor. Soc., 132, 1179–1203, http://dx.doi.org/10.1256/qj.05.51, 2006.

Dörnbrack, A., Pitts, M. C., Poole, L. R., Orsolini, Y. J., Nishii, K., and Nakamura, H.: The 2009–2010 Arctic stratospheric winter –general evolution, mountain waves and predictability of an operational weather forecast model, Atmos. Chem. Phys., 12, 3659–3675, doi:10.5194/acp-12-3659-2012, http://www.atmos-chem-phys.net/12/3659/2012/, 2012.

El Amraoui, L., Semane, N., Peuch, V. H., and Santee, M. L.: Investigation of dynamical processes in the polar stratospheric vortex during the unusually cold winter 2004/2005, Geophys. Res. Lett., 35, L03 803, doi:10.1029/2007GL031251, http://dx.doi.org/10.1029/2007GL031251, 2008.

Frisk, U., Hagström, M., Ala-Laurinaho, J., Andersson, S., Berges, J. C., Chabaud, J. P., Dahlgren, M., Emrich, A., Florén, H. G., Florin, G., Fredrixon, M., Gaier, T., Haas, R., Hirvonen, T., Hjalmarsson, Å., Jakobsson, B., Jukkala, P., Kildal, P. S., Kollberg, E., Lassing, J., Lecacheux, A., Lehikoinen, P., Lehto, A., Mallat, J., Marty, C., Michet, D., Narbonne, J., Nexon, M., Olberg, M., Olofsson, A. O. H., Olofsson, G., Origné, A., Petersson, M., Piironen, P., Pons, R., Pouliquen, D., Ristorcelli, I., Rosolen, C., Rouaix, G., Räisänen, A. V., Serra, G., Sjöberg, F., Stenmark, L., Torchinsky, S., Tuovinen, J., Ullberg, C., Vinterhav, E., Wadefalk, N., Zirath, H., Zimmermann, P., and Zimmermann, R.: The Odin satellite, A&A, 402, L27–L34, doi:10.1051/0004-6361:20030335, http://dx.doi.org/10.1051/0004-6361:20030335, 2003.

Grooß, J. U. and Müller, R.: Simulation of ozone loss in Arctic winter 2004/2005, Geophys. Res. Lett., 34, L05 804, doi:10.1029/2006GL028901, http://dx.doi.org/10.1029/2006GL028901, 2007.

Hommel, R., Eichmann, K. U., Aschmann, J., Bramstedt, K., Weber, M., von Savigny, C., Richter, A., Rozanov, A., Wittrock, F., Khosrawi, F., Bauer, R., and Burrows, J. P.: Chemical ozone loss and ozone mini-hole event during the Arctic winter 2010/2011 as observed by SCIAMACHY and GOME-2, Atmos. Chem. Phys., 14, 3247–3276, doi:10.5194/acp-14-3247-2014, http://www.atmos-chem-phys.net/14/3247/2014/, 2014.

Jackson, D. R. and Orsolini, Y. J.: Estimation of Arctic ozone loss in winter 2004/05 based on assimilation of EOS MLS and SBUV/2 observations, Q. J. Roy. Meteor. Soc., 134, 1833–1841, doi:10.1002/qj.316, http://dx.doi.org/10.1002/qj.316, 2008.

Jones, A., Murtagh, D., Urban, J., Eriksson, P., and Rosevall, J.: Intercomparison of Odin/SMR ozone measurements with MIPAS and balloonsonde data, Can. J. Phys., 85, 1111–1123, http://www.ingentaconnect.com/content/nrc/cjp/2007/00000085/00000011/art00003, 2007.

Kasai, Y., Sagawa, H., Kreyling, D., Dupuy, E., Baron, P., Mendrok, J., Suzuki, K., Sato, T. O., Nishibori, T., Mizobuchi, S., Kikuchi, K., Manabe, T., Ozeki, H., Sugita, T., Fujiwara, M., Irimajiri, Y., Walker, K. A., Bernath, P. F., Boone, C., Stiller, G., von Clarmann, T., Orphal, J., Urban, J., Murtagh, D., Llewellyn, E. J., Degenstein, D., Bourassa, A. E., Lloyd, N. D., Froidevaux, L., Birk, M., Wagner, G.,

Schreier, F., Xu, J., Vogt, P., Trautmann, T., and Yasui, M.: Validation of stratospheric and mesospheric ozone observed by SMILES from International Space Station, Atmos. Meas. Tech., 6, 2311–2338, doi:10.5194/amt-6-2311-2013, http://www.atmos-meas-tech.net/6/2311/2013/, 2013.

Khosrawi, F., Urban, J., Pitts, M. C., Voelger, P., Achtert, P., Kaphlanov, M., Santee, M. L., Manney, G. L., Murtagh, D., and Fricke, K. H.: Denitrification and polar stratospheric cloud formation during the Arctic winter 2009/2010, Atmos. Chem. Phys., 11, 8471–8487, doi:10.5194/acp-11-8471-2011, http://www.atmos-chem-phys.net/11/8471/2011/, 2011.

Kikuchi, K., Nishibori, T., Ochiai, S., Ozeki, H., Irimajiri, Y., Kasai, Y., Koike, M., Manabe, T., Mizukoshi, K., Murayama, Y., Nagahama, T., Sano, T., Sato, R., Seta, M., Takahashi, C., Takayanagi, M., Masuko, H., Inatani, J., Suzuki, M., and Shiotani, M.: Overview and early results of the Superconducting Submillimeter-Wave Limb-Emission Sounder (SMILES), J. Geophys. Res., 115, D23 306, doi:10.1029/2010JD014379, http://dx.doi.org/10.1029/2010JD014379, 2010.

Konopka, P., Engel, A., Funke, B., Müller, R., Grooß, J.-U., Günther, G., Wetter, T., Stiller, G., von Clarmann, T., Glatthor, N., Oelhaf, H., Wetzel, G., López-Puertas, M., Pirre, M., Huret, N., and Riese, M.: Ozone loss driven by nitrogen oxides and triggered by stratospheric warmings can outweigh the effect of halogens, J. Geophys. Res., 112, D05 105, doi:10.1029/2006JD007064, http://dx.doi.org/10.1029/2006JD007064, 2007.

Kuttippurath, J. and Nikulin, G.: A comparative study of the major sudden stratospheric warmings in the Arctic winters 2003/2004–2009/2010, Atmos. Chem. Phys., 12, 8115–8129, doi:10.5194/acp-12-8115-2012, http://www.atmos-chem-phys.net/12/8115/2012/, 2012.

Kuttippurath, J., Godin-Beekmann, S., Lefèvre, F., and Goutail, F.: Spatial, temporal, and vertical variability of polar stratospheric ozone loss in the Arctic winters 2004/2005–2009/2010, Atmos. Chem. Phys., 10, 9915–9930, doi:10.5194/acp-10-9915-2010, http://www.atmos-chem-phys.net/10/9915/2010/, 2010.

Lait, L. R.: An Alternative Form for Potential Vorticity, J. Atmos. Sci., 51, 1754–1759, doi:10.1175/1520-0469(1994)051⟨1754:AAFFPV⟩2.0.CO;2, http://dx.doi.org/10.1175/1520-0469(1994)051⟨1754:AAFFPV⟩2.0.CO;2, 1994.

Lambert, A., Read, W. G., Livesey, N. J., Santee, M. L., Manney, G. L., Froidevaux, L., Wu, D. L., Schwartz, M. J., Pumphrey, H. C., Jimenez, C., Nedoluha, G. E., Cofield, R. E., Cuddy, D. T., Daffer, W. H., Drouin, B. J., Fuller, R. A., Jarnot, R. F., Knosp, B. W., Pickett, H. M., Perun, V. S., Snyder, W. V., Stek, P. C., Thurstans, R. P., Wagner, P. A., Waters, J. W., Jucks, K. W., Toon, G. C., Stachnik, R. A., Bernath, P. F., Boone, C. D., Walker, K. A., Urban, J., Murtagh, D., Elkins, J. W., and Atlas, E.: Validation of the Aura Microwave Limb Sounder middle atmosphere water vapor and nitrous oxide measurements, J. Geophys. Res., 112, D24S36, doi:10.1029/2007JD008724, http://dx.doi.org/10.1029/2007JD008724, 2007.

Murtagh, D., Frisk, U., Merino, F., Ridal, M., Jonsson, A., Stegman, J., Witt, G., Eriksson, P., Jiménez, C., Megie, G., Noë, J. d. l., Ricaud, P., Baron, P., Pardo, J. R., Hauchcorne, A., Llewellyn, E. J., Degenstein, D. A., Gattinger, R. L., Lloyd, N. D., Evans, W. F., McDade, I. C., Haley, C. S., Sioris, C., Savigny, C. v., Solheim, B. H., McConnell, J. C., Strong, K., Richardson, E. H., Leppelmeier, G. W., Kyrölä, E., Auvinen, H., and Oikarinen, L.: An overview of the Odin atmospheric mission, Can. J. Phys., 80, 309–319, doi:10.1139/p01-157, http://dx.doi.org/10.1139/p01-157, 2002.

Prather, M. J.: Numerical Advection by Conservation of Second-Order Moments, J. Geophys. Res., 91, 6671–6681, doi:10.1029/JD091iD06p06671, http://dx.doi.org/10.1029/JD091iD06p06671, 1986.

WMO: Scientific Assessment of Ozone Depletion: 2010, Global Ozone Research and Monitoring Project-Report No. 52, 516pp., Geneva, Switzerland, 2011.

Rodgers, C. D.: Inverse methods for atmospheric sounding: Theory and Practice, Series on Atmospheric, Oceanic and Planetary Physics–Vol. 2, Singapore, World Scentic, 2000.

Rösevall, J. D., Murtagh, D. P., and Urban, J.: Ozone depletion in the 2006/2007 Arctic winter, Geophys. Res. Lett., 34, L21 809, doi:10.1029/2007GL030620, http://dx.doi.org/10.1029/2007GL030620, 2007a.

Rösevall, J. D., Murtagh, D. P., Urban, J., and Jones, A. K.: A study of polar ozone depletion based on sequential assimilation of satellite data from the ENVISAT/MIPAS and Odin/SMR instruments, Atmos. Chem. Phys., 7, 899–911, doi:10.5194/acp-7-899-2007, http://www.atmos-chem-phys.net/7/899/2007/, 2007b.

Rösevall, J. D., Murtagh, D. P., Urban, J., Feng, W., Eriksson, P., and Brohede, S.: A study of ozone depletion in the 2004/2005 Arctic winter based on data from Odin/SMR and Aura/MLS, J. Geophys. Res., 113, D13 301, doi:10.1029/2007JD009560, http://dx.doi.org/10.1029/2007JD009560, 2008.

Scherhag, R.: Die explosionsartige Stratosphärenerwärmung des Spätwinters 1951/52, Berichte des Deutschen Wetterdienstes, 38, 51–63, 1952.

Solomon, S.: The mystery of the Antarctic "Ozone Hole", Rev. Geophys., 26, 131–148, doi:10.1029/RG026i001p00131, http://dx.doi.org/10.1029/RG026i001p00131, 1988.

Solomon, S.: Stratospheric ozone depletion: A review of concepts and history, Rev. Geophys., 37, 275–316, doi:10.1029/1999RG900008, http://dx.doi.org/10.1029/1999RG900008, 1999.

Sonkaew, T., von Savigny, C., Eichmann, K. U., Weber, M., Rozanov, A., Bovensmann, H., Burrows, J. P., and Grooß, J. U.: Chemical ozone losses in Arctic and Antarctic polar winter/spring season derived from SCIAMACHY limb measurements 2002–2009, Atmos. Chem. Phys., 13, 1809–1835, doi:10.5194/acp-13-1809-2013, http://www.atmos-chem-phys.net/13/1809/2013/, 2013.

Søvde, O. A., Orsolini, Y. J., Jackson, D. R., Stordal, F., Isaksen, I. S. A., and Rognerud, B.: Estimation of Arctic O3 loss during winter 2006/2007 using data assimilation and comparison with a chemical transport model, Q. J. Roy. Meteor. Soc., 137, 118–128, doi:10.1002/qj.740, http://dx.doi.org/10.1002/qj.740, 2011.

Strong, K., Wolff, M. A., Kerzenmacher, T. E., Walker, K. A., Bernath, P. F., Blumenstock, T., Boone, C., Catoire, V., Coffey, M., De Mazière, M., Demoulin, P., Duchatelet, P., Dupuy, E., Hannigan, J., Höpfner, M., Glatthor, N., Griffith, D. W. T., Jin, J. J., Jones, N., Jucks, K., Kuellmann, H., Kuttippurath, J., Lambert, A., Mahieu, E., McConnell, J. C., Mellqvist, J., Mikuteit, S., Murtagh, D. P., Notholt, J., Piccolo, C., Raspollini, P., Ridolfi, M., Robert, C., Schneider, M., Schrems, O., Semeniuk, K., Senten, C., Stiller, G. P., Strandberg, A., Taylor, J., Tétard, C., Toohey, M., Urban, J., Warneke, T., and Wood, S.: Validation of ACE-FTS N2O measurements, Atmos. Chem. Phys., 8, 4759–4786, doi:10.5194/acp-8-4759-2008, http://www.atmos-chem-phys.net/8/4759/2008/, 2008.

Urban, J., Lautié, N., Le Flochmoën, E., Jiménez, C., Eriksson, P., de La Noë, J., Dupuy, E., Ekström, M., El Amraoui, L., Frisk, U., Murtagh, D., Olberg, M., and Ricaud, P.: Odin/SMR limb observations of stratospheric trace gases: Level 2 processing of ClO, N2O, HNO3, and O3, J. Geophys. Res., 110, D14 307, doi:10.1029/2004JD005741, http://dx.doi.org/10.1029/2004JD005741, 2005a.

Urban, J., Lautié, N., Le Flochmoën, E., Jiménez, C., Eriksson, P., de La Noë, J., Dupuy, E., El Amraoui, L., Frisk, U., Jégou, F., Murtagh, D., Olberg, M., Ricaud, P., Camy-Peyret, C., Dufour, G., Payan, S., Huret, N., Pirre, M., Robinson, A. D., Harris, N. R. P., Bremer, H., Kleinböhl, A., Küllmann, K., Künzi, K.,

Kuttippurath, J., Ejiri, M. K., Nakajima, H., Sasano, Y., Sugita, T., Yokota, T., Piccolo, C., Raspollini, P., and Ridolfi, M.: Odin/SMR limb observations of stratospheric trace gases: Validation of N2O, J. Geophys. Res., 110, D09 301, doi:10.1029/2004JD005394, http://dx.doi.org/10.1029/2004JD005394, 2005b.

Wohltmann, I., Wegner, T., Müller, R., Lehmann, R., Rex, M., Manney, G. L., Santee, M. L., Bernath, P., Sumińska-Ebersoldt, O., Stroh, F., von Hobe, M., Volk, C. M., Hösen, E., Ravegnani, F., Ulanovsky, A., and Yushkov, V.: Uncertainties in modelling heterogeneous chemistry and Arctic ozone depletion in the winter 2009/2010, Atmos. Chem. Phys., 13, 3909–3929, doi:10.5194/acp-13-3909-2013, http://www.atmos-chem-phys.net/13/3909/2013/, 2013.

Table 1: Typical specification of the observations

Parameters	SMILES	SMR
Orbit	non-sun-synchronous orbit	sun-synchronous orbit
Inclination angle	51.6°	98°
Altitude	340–360 km	about 600 km
Latitude coverage	38°S– 65°N	82.5°S– 82.5°N
Parameters (data sampling)		
Measurement geometry	limb scan	limb scan
Scan altitude	-20–120 km	7–72 km
Vertical sampling interval	about 2 km (0.056°)	1.5 km (0.875 sec) below 50 km
		6 km (3.5 sec) for the mesosphere
Number of samples	∼1630 scans per day	∼900 scans per day
Nominal data sampling	∼100 scans per orbit	∼60 scans per orbit

Table 2: Description of the calculations

Condition	Value
Time period	2009-12-01 ∼ 2010-03-31
Initialisation	1 month (2009-11-01 ∼ 2009-12-01)
Altitude range (EPT)	450K ∼ 900K (25K resolution)
Measurement Response	≥0.85

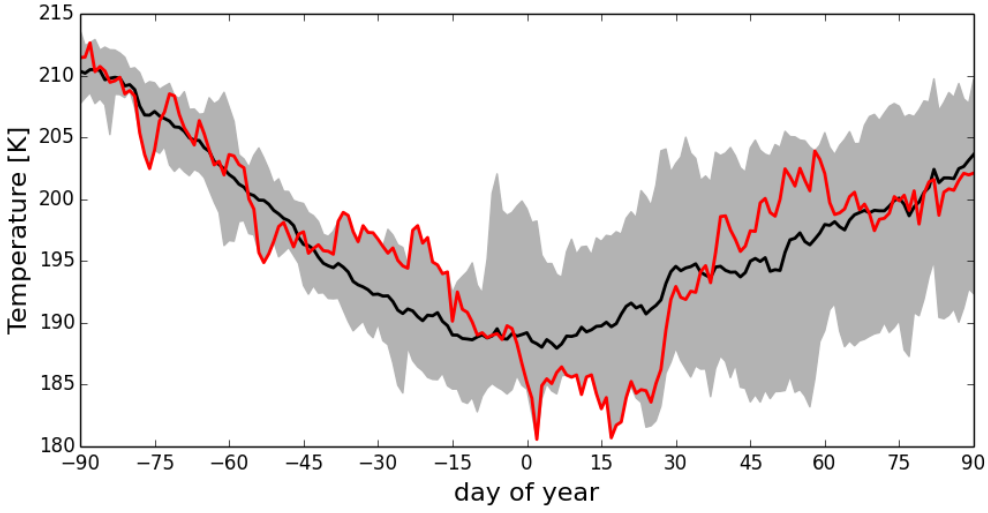

Fig. 1: Minimum ECMWF temperature, T_{min} [K], at a potential temperature of 500K inside the area where the equivalent latitude (EQL) is greater than 70 °, corresponding to the area inside the Arctic polar vortex, as function of days of year (1 January refers to 0). The black solid line shows the mean value from 2001 to 2012. The red line is the T_{min} temporal evolution from 1 October 2009 to 31 March 2010. The shaded area encompasses the minimum/maximum T_{min} between 2001 and 2011.

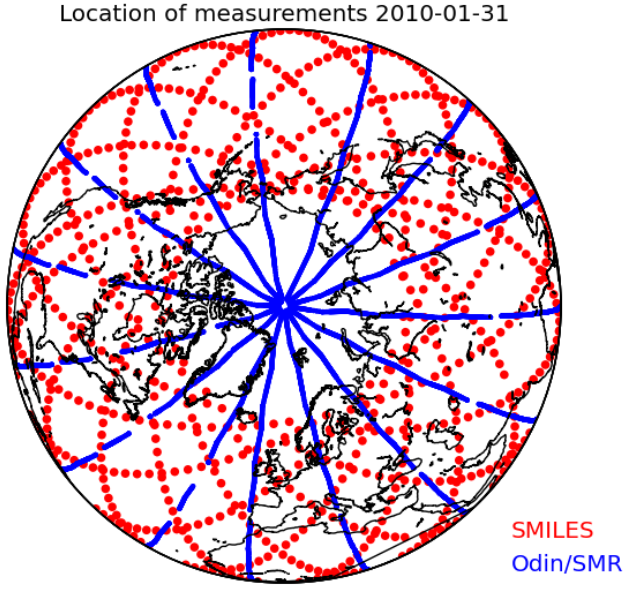

Fig. 2: Geographical distributions of ozone observations from SMILES and Odin/SMR on 2010-01-31.

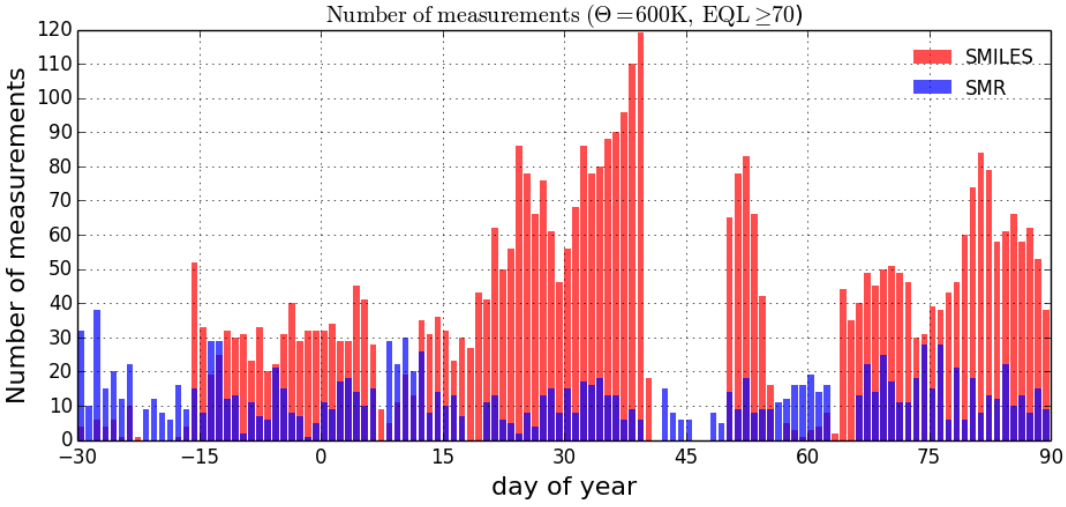

Fig. 3: The number of measurements inside the area where the equivalent latitude is greater than 70°N on a potential temperature surface of 500K against day of year (1 January refers to 0). Note that only measurements with measurement response above than a threshold of 0.85 are considered.

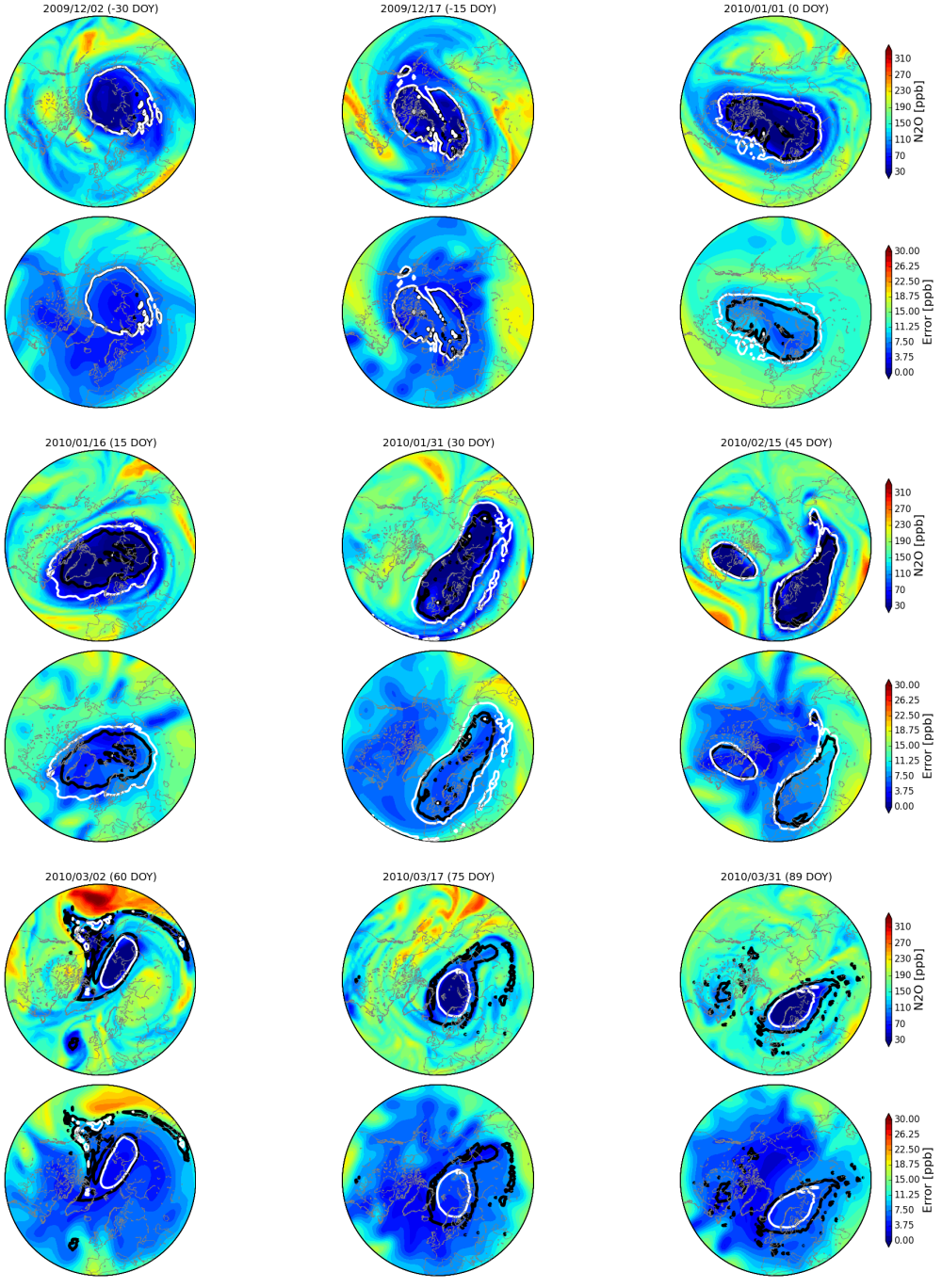

Fig. 4: Modeled N_2O fields with assimilation of SMR data (top) and their error fields (bottom) on selected dates at 600K level. The number in the bracket indicates the days of year. The contour lines indicate the vortex edge described with two criteria. The black line is based on the equivalent latitude ($=70°$N) and the white line is based on Lait's potential vorticity ($= 38\mathrm{PVU} = 3.8 \times 10^{-6}\mathrm{Km^2kg^{-1}s^{-1}}$).

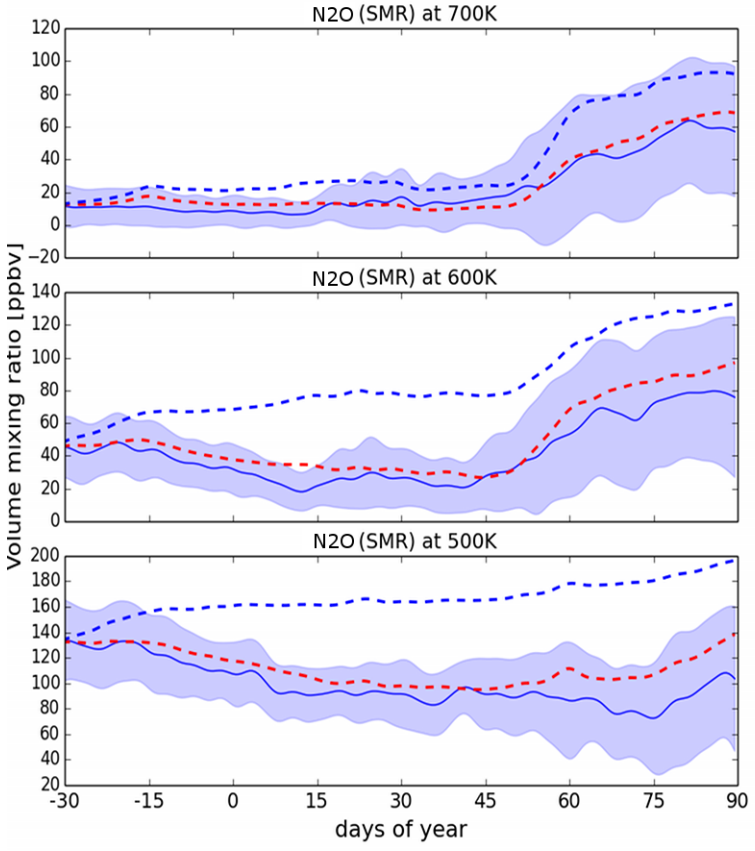

Fig. 5: Time series of the vortex mean N_2O mixing ratio in the DIAMOND model at selected potential temperature levels. The blue solid line shows the average inside the area where the equivalent latitude is $\geq 70°$N, calculated from the assimilated field of Odin N_2O. The dashed lines show vortex means of predictions initiated on December 1, using the 2D off-line advection model including vertical transport (red) and the advection model without any vertical transport (blue). The shaded area indicates the estimated error (more detail can be seen in Figure 6). All data are smoothed over 3 days.

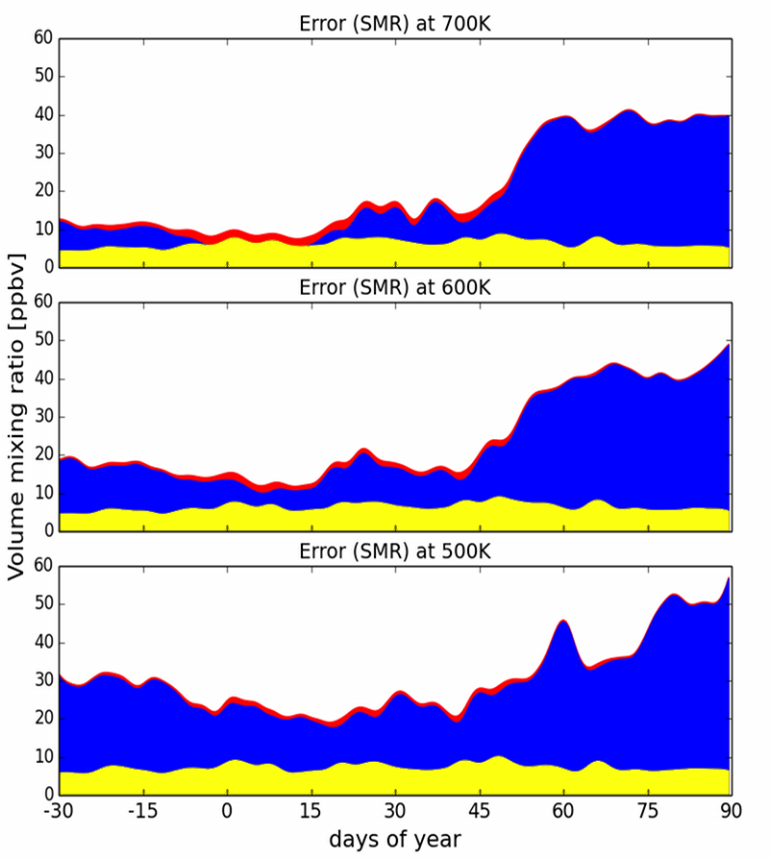

Fig. 6: The estimated uncertainty of the vortex mean of N_2O. The blue area shows the standard deviation (σ) inside the vortex (EQL $\geq$ 70). The yellow area shows the vortex mean of the error fields ($\hat{E}$). Finally, the red area indicates the total estimated error, which has been calculated as $\sqrt{\sigma^2 + \hat{E}^2}$ and is shown as uncertainties in Figure 5. All data are smoothed over 3 days.

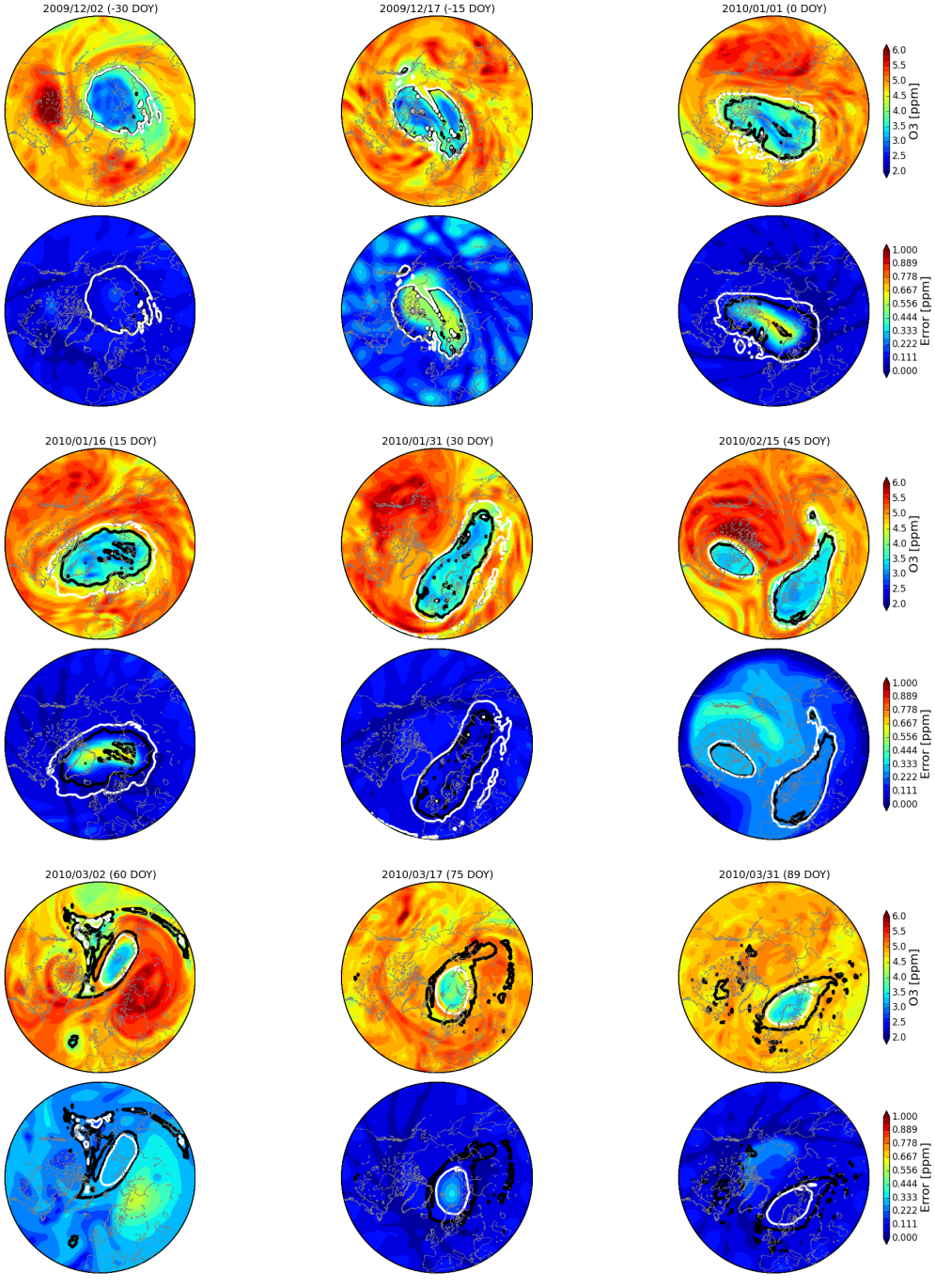

Fig. 7: Same as figure 4 but for ozone derived from SMILES.

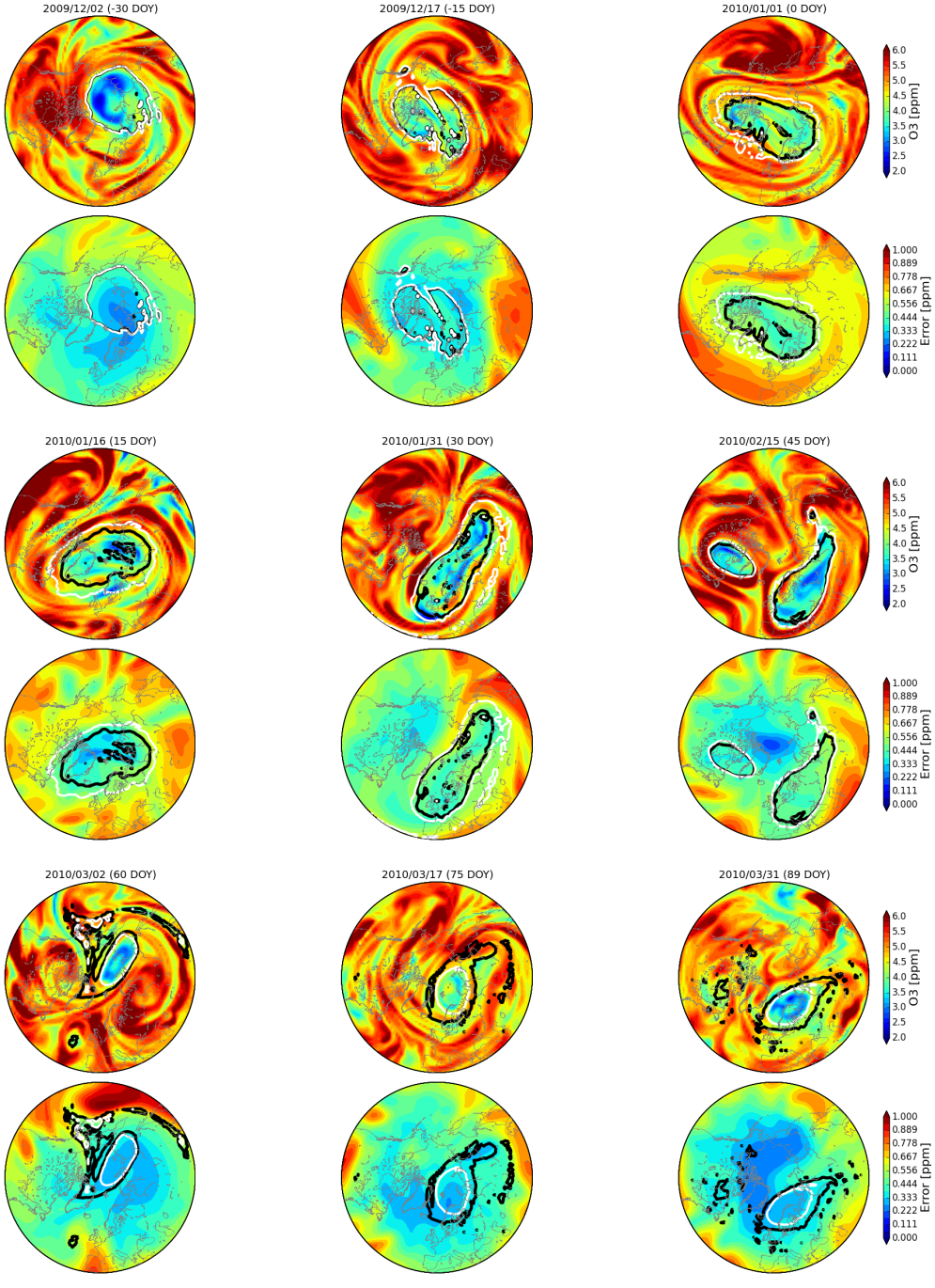

Fig. 8: Same as figure 4 but for ozone derived from SMR.

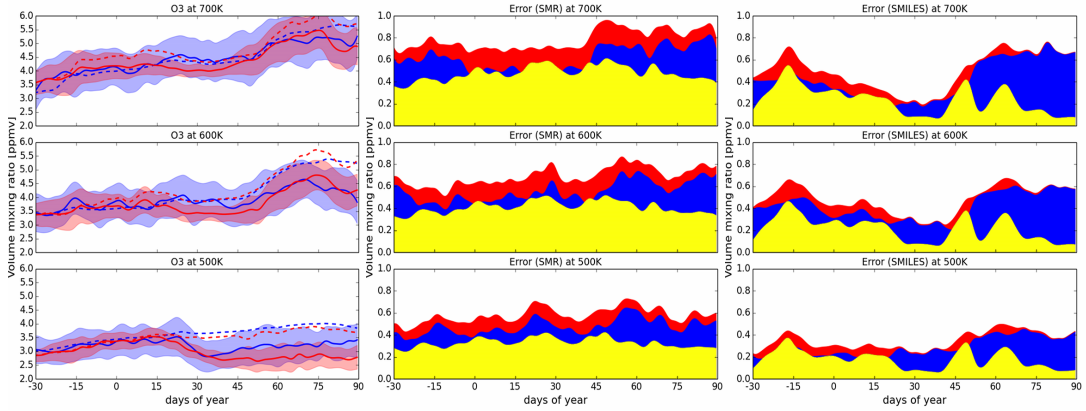

Fig. 9: (Left panels) Same as figure 5 but for ozone from SMR (blue) and SMILES (red). (Middle panels) Same as figure 6 but for ozone from SMR. (Right panels) Same as figure 6 but for ozone from SMILES.

(a) Ozone loss SMR 501GHz

(b) Ozone loss SMILES

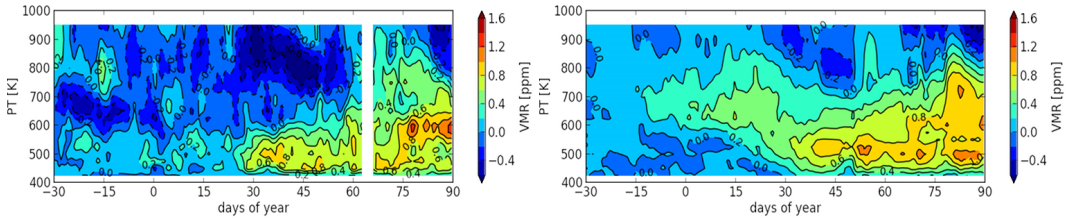

(c) ClO (daytime) SMR 501GHz

(d) ClO (nighttime) SMR 501GHz

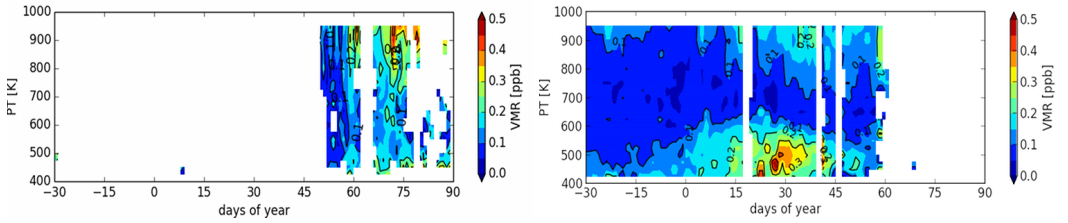

(e) Cumulative sun exposure

(f) Minimum ECMWF temperature

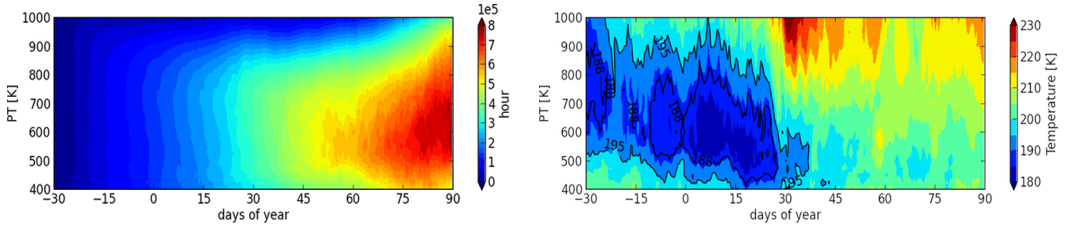

(g) Area with temperatures below 195K

(h) Area with temperatures below 188K

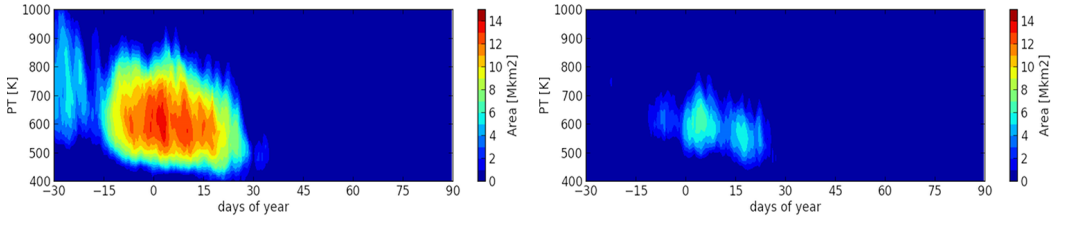

Fig. 10: Vortex averages of several parameters in the area where equivalent latitudes are larger than 70° as a function of time (days from 1 Jan 2010) and isentropic levels between 400K and 1000K. (a,b) Vortex mean ozone loss derived from SMR and SMILES, respectively. (c,d) Vortex mean ClO retrieved from SMR in daytime and nighttime, respectively. (e) Cumulative sun exposure time of the polar vortex. (f) Minimum air temperature inside the vortex derived from ECMWF. (g,h) Areas where the temperature is below T_{NAT} and T_{ice}, respectively.

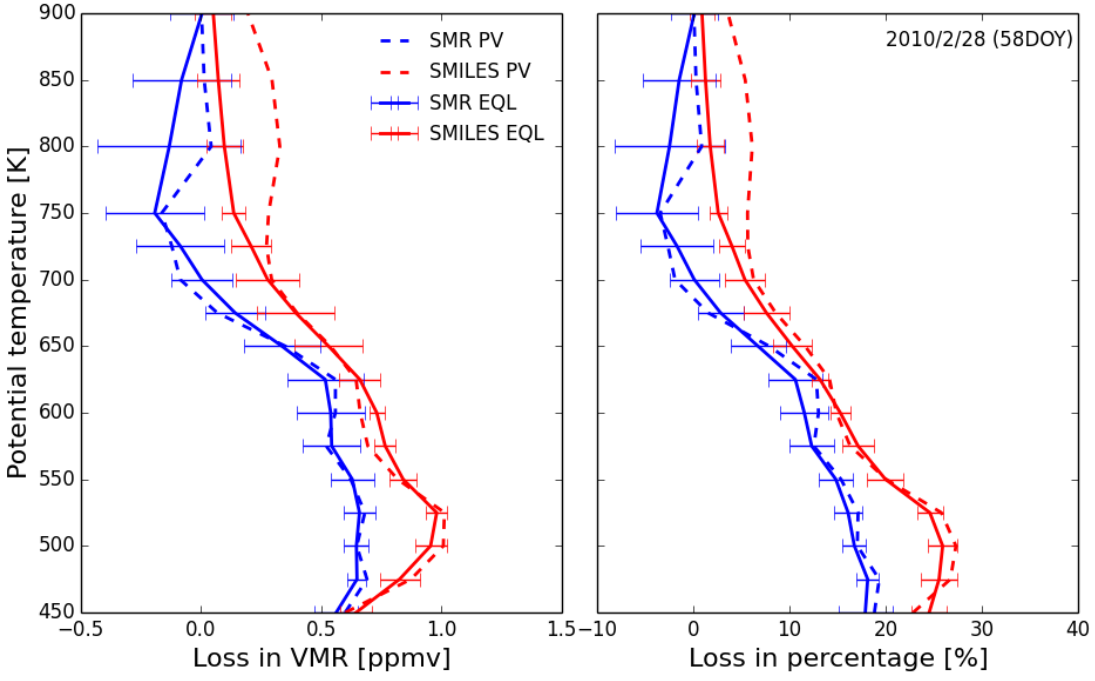

Fig. 11: Vertical profiles of accumulated ozone loss as of 28 February 2010 from 1 December 2009. Loss was derived by subtracting the passive ozone from the assimilated ozone. The error bars are given as the standard deviation of derived daily ozone loss inside the vortex for the period of $\pm$ 3 days from 28 February 2010. The left panel shows loss in VMR, and the right panel shows relative losses in percent. The solid lines indicate losses with using the EQL criteria for the vortex edge ($\geq$ 70°N) while dashed lines show losses obtained using the modified PV criteria ($\geq$ 38PVU).

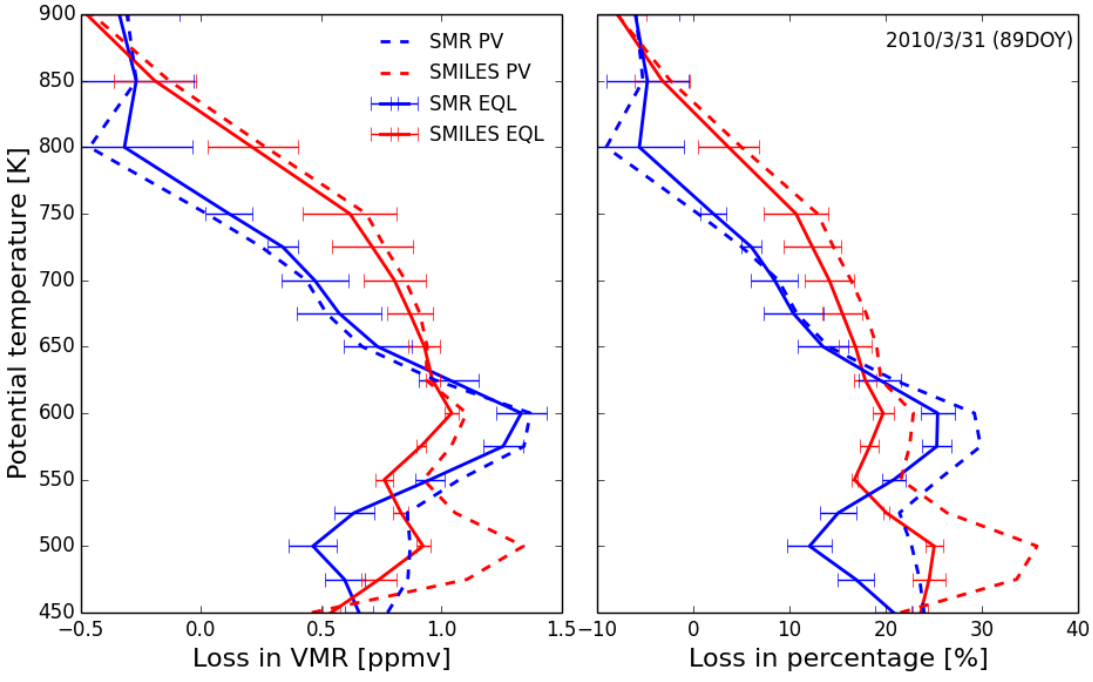

Fig. 12: Same as figure 11 but for 31 March 2010.